Angewandte Chemie
Eine Zeitschrift der Gesellschaft Deutscher Chemiker

Supporting Information

Highly Active Oxidation Catalysts through Confining Pd Clusters on CeO_2 Nano-Islands

*D. Gashnikova, F. Maurer, E. Sauter, S. Bernart, J. Jelic, P. Dolcet, C. B. Maliakkal, Y. Wang, C. Wöll, F. Studt, C. Kübel, M. Casapu, J.-D. Grunwaldt**

License: CC BY 4.0 International - Creative Commons, Attribution

Supporting Information

Highly active oxidation catalysts through confining Pd clusters on CeO_2 nano-islands

Daria Gashnikova[1], *Florian Maurer*[1], *Eric Sauter*[2], *Sarah Bernart*[3], *Jelena Jelic*[3], *Paolo Dolcet*[1], *Carina B. Maliakkal*[4], *Yuemin Wang*[2], *Christof Wöll*[2], *Felix Studt*[3], *Christian Kübel*[4,5], *Maria Casapu*[1], *Jan-Dierk Grunwaldt*[1,3,*]

[1] Institute for Chemical Technology and Polymer Chemistry (ITCP), Karlsruhe Institute of Technology (KIT), Engesserstraße 20, 76131 Karlsruhe, Germany

[2] Institute of Functional Interfaces (IFG), Karlsruhe Institute of Technology (KIT), Hermann-von-Helmholtz-Platz 1, 76344 Eggenstein-Leopoldshafen, Germany

[3] Institute of Catalysis Research and Technology (IKFT), Karlsruhe Institute of Technology (KIT), Hermann-von-Helmholtz-Platz 1, 76344 Eggenstein-Leopoldshafen, Germany

[4] Institute of Nanotechnology (INT) and Karlsruhe Nano Micro Facility (KNMFi), Karlsruhe Institute of Technology (KIT), Hermann-von-Helmholtz-Platz 1, 76344 Eggenstein-Leopoldshafen, Germany

[5] Institute of Materials Research, Technical University Darmstadt (TUDa), Peter-Grünberg-Straße 2, 64287 Darmstadt, Germany

Corresponding author: *grunwaldt@kit.edu

Table of contents

Experimental section

Catalyst preparation

The catalysts were synthesised by flame spray pyrolysis (FSP) using an in-house built setup described in more detail in ref. [34].

The synthesis of the double nozzle-flame prepared samples 0.5% Pd/Al_2O_3 and 0.5% Pd/CeO_2 was conducted as follows. For the 0.5% Pd/Al_2O_3 catalyst, the corresponding amount (45.7 mg) of palladium acetylacetonate (ACROS organics, 35% Pd) was dissolved in 250 mL xylene, whereas the second precursor solution contained 20.2 g of aluminium acetylacetonate (Sigma Aldrich, ≥98%) in 250 mL of HOAc/MeOH (1:1). In case of 0.5% Pd/CeO_2, palladium and cerium precursors (15.3 mg and 72.1 g, respectively) were dissolved separately in 250 mL xylene.

For 0.5% Pd/5% CeO_2-Al_2O_3, 47.4 mg palladium acetylacetonate and 1.12 g cerium ethylhexanoate (Alfa Aesar, 12% Ce) were dissolved in 250 mL of xylene. The alumina precursor solution consisting of 19.9 g of aluminium acetylacetonate (Sigma Aldrich, ≥98%) in 250 mL of HOAc/MeOH was sprayed separately from palladium and cerium solution. Due to a low solubility of aluminium acetylacetonate in xylene, a 1:1 mixture of acetic acid and methanol was used as a solvent. The catalyst with higher CeO_2 content (0.5 %Pd/10% CeO_2-Al_2O_3) was synthesized analogously. The total precursor concentration was always fixed to 0.125 M.

In the next step, the solutions were dosed via capillary tubes with a flow of 5 mL min^{-1} and dispersed with a O_2 flow of 5 L min^{-1} at a back pressure of 3 bar. Two nozzles were positioned at an angle of 120° and the distance between the nozzles was fixed to 10.6 cm. The ignition of the sprays took place in an annular CH_4 flame (0.75 L min^{-1} CH_4 and 1.6 L min^{-1} O_2). The gas flows were adjusted by mass flow controllers (Bronkhorst). The formed nanoparticles were collected on water-cooled glass fibre filters (Glasfaser Filter GF 6, Whatman) placed in a cylindrical filter holder connected to a vacuum pump. The catalyst powder was collected from the filters and calcined at 500 °C for 5 h in order to remove remaining precursor residues.

For the synthesis of Pd/CeO_2 catalysts with a nominal weight loading of 0.5% and 1.0% Pd using a single flame configuration, the adjusted amount of precursors was dissolved in 500 mL xylene. Other synthesis parameters were kept unchanged to ensure the comparability of the synthesis methods. The samples prepared in a single flame configuration are denoted as 0.5% Pd/CeO_2-SF and 1.0% Pd/CeO_2-SF, respectively.

A standard 1.0% Pd/Al_2O_3 catalyst was prepared *via* incipient wetness impregnation and used for comparison in this study. During the synthesis, 200 mg tetraamminepalladium (II) nitrate solution (abcr, 5.0% Pd) in 0.3 mL water was added dropwise to the 0.99 g Al_2O_3 support. The obtained powder was dried at 70 °C for 1 h and calcined at 500 °C for 5 h.

Catalytic tests

For catalytic tests, 100 mg of the catalyst (sieve fraction of 125-250 µm) was diluted with 900 mg quartz (Sigma Aldrich, washed and calcined for analysis) and placed in a tubular quartz reactor with an inner diameter of 8 mm. The total gas flow was set to 500 mL min^{-1} to obtain a WHSV of 300 L $(g_{cat} \cdot h)^{-1}$ or 60 000 L $(g_{noble\ metal} \cdot h)^{-1}$. In case of 1.0% Pd/CeO_2-SF, the amount of the catalyst, dilution and the total gas flow were adjusted to the noble metal loading keeping an overall reactor loading of 1 g. The temperature inside the reactor was monitored by two thermocouples placed up- and downstream of the catalyst bed. The gas composition at the reactor outlet was continuously analysed using a Fourier transform infrared spectrometer (Multigas 2030 FTIR Continuous Gas Analyser, MKS Instruments).

For evaluation of the catalytic activity, the catalyst was heated up to 500 °C with a heating ramp of 5 K min^{-1} in a mixture of 1000 ppm CO, 8 vol.% O_2 and N_2 as balance. The temperature was held for 1 h before the catalyst was cooled to room temperature. The gas flows were adjusted *via* mass flow controllers (Bronkhorst). To evaluate the catalyst stability, three consecutive cycles to 500 °C were performed.

***Ex situ* Characterization**

ICP-OES: The elemental composition of the samples and palladium loading were determined by inductively coupled plasma optical emission spectroscopy (ICP-OES) using an iCAP 7600 DUO (Thermo-Fisher-Scientific) spectrometer at the Institute for Applied Materials (IAM-AWP) at Karlsruhe Institute of Technology (KIT).

BET: The specific surface area was determined by N_2 physisorption according to the Brunauer-Emmett-Teller[35] (BET) method on the BELSORP-mini II (BEL Inc.). Prior to the analysis, the samples were degassed under reduced pressure at 300 °C for 2 h.

XRD: Powder X-ray diffraction (XRD) patterns were recorded using a Bruker Advance D8 diffractometer with nickel-filtered $CuK_{\alpha 1}$ radiation (wavelength = 0.154 nm) in the 2θ range between 10 and 120° with a step size of 0.016° and an acquisition time of 3 s per point.

TEM: High angle annular dark field scanning transmission electron microscopy (HAADF-STEM) images and energy dispersive X-ray spectroscopy (EDXS) mappings were

acquired with a FEI Themis Z or FEI Themis 300 electron microscope operated at 300 keV at the KNMF located at the Institute of Nanotechnology (INT) at KIT.

EXAFS: *Ex situ* extended X-ray absorption fine structure (EXAFS) spectra at the Pd K-edge were collected at the CAT-ACT beamline[36] in transmission mode. A double crystal monochromator (DCM) with Si(311) crystals was used to tune the energy of the incident X-ray beam. The size of the X-ray beam was set to 3 mm in width and 3 mm in height. Prior the *ex situ* EXAFS measurements, the samples were diluted with cellulose and pressed to a pellet. For each sample, two spectra were recorded, which were merged and used for the EXAFS fitting. A *k*-range of 2.5-10.0 $Å^{-1}$ was selected for all samples, whereas the EXAFS fitting was performed in an R-range of 1.1-3.4 Å.

Operando XAS

Operando X-ray absorption spectroscopy (XAS) spectra at the Pd-K-edge were recorded in fluorescence mode using a 35 pixels HPGe fluorescence detector (Canberra) at the beamline SAMBA at the synchrotron radiation facility SOLEIL (Saint-Aubin, France). Si(220) channel-cut crystals were used for the measurements. The size of the beam was set to 0.2 mm in height and 1.5 mm in width. For the *operando* investigations, 7.5 mg of the catalyst (100-200 µm) were loaded in a quartz capillary microreactor (1.5 mm outer diameter, 0.01 mm wall thickness) and placed in a high-temperature cell[37]. Gases were supplied *via* mass flow controllers (Bronkhorst). The total gas flow was set to 75 mL min^{-1} yielding a WHSV of 120 000 L $(g_{noble\ metal} \cdot h)^{-1}$. The catalysts were heated and cooled with 5 K min^{-1} during the experiments. The gas concentration was monitored at the reactor outlet on-line using a mass spectrometer (Omnistar, Pfeiffer Vacuum) and a Fourier-transform infrared spectrometer (Multigas 2030 FTIR Continuous Gas Analyser, MKS Instruments). For the linear combination analysis (LCA), the following internal references were used: Spectra of Pd/CeO_2 recorded at room temperature in He before and after CO-TPR were used as oxidized and reduced references respectively.

Temperature programmed reduction (TPR) was performed using 1000 ppm CO or 2% H_2 in He as a reducing agent. During TPR, the catalyst was heated to 400 °C in reducing mixture with a heating rate of 5 K min^{-1}.

For CO oxidation experiments, the catalyst was heated up to 500 °C without any pre-treatment with 5 K min^{-1} in reaction mixture (1000 ppm CO, 10 vol.% O_2 and He). After 1 h at 500 °C the catalyst was cooled in reaction mixture to room temperature and the whole cycle was repeated one more time.

DRIFTS

Diffuse reflectance infrared Fourier transform spectroscopy (DRIFTS) measurements were performed on a VERTEX 70 Fourier transform infrared spectrometer (Bruker) equipped with a Praying Mantis diffuse reflection optics (Harrick) and a liquid nitrogen-cooled mercury cadmium telluride detector. For the DRIFTS measurements, the catalyst was diluted with CaF_2 in a ratio of 1:4. In the next step, the diluted catalyst was pressed and sieved in a desired sieve fraction (100-200 µm). The sieved catalyst powder was then placed in a high-temperature *in situ* cell (Harrick) covered with a CaF_2 window. The temperature in the reactor is controlled by two heating cartridges inside the cell and by a water-cooling system. Note that a strong temperature gradient existing in the DRIFTS cell[38] needs to be taken into account when interpreting the data. Therefore, a correlation between the temperature set point and an actual temperature was estimated prior the experiments with an ImageIR® 8300 camera (InfraTec) by monitoring the temperature on the surface of catalyst bed (used calibrations: M1x(30-150) and M1x(175-400) for temperatures below and above 150 °C). The temperature specification in the manuscript is based on the values observed with the ImageIR ® 8300 camera.

Prior the CO adsorption experiments, the catalysts were oxidatively pre-treated at 350 °C for 1 h in 10% O_2/Ar (200 mL min^{-1}) at ambient pressure. Afterwards, the cell was stepwise cooled to the desired temperature (350-50 °C) where a background spectrum for a certain temperature was recorded in 10% O_2/Ar with a flow of 200 mL min^{-1}. Subsequently, the DRIFTS experiments in reaction mixture (1000 ppm CO; 10% O_2; Ar; 200 mL min^{-1}) were performed. The gas composition at the cell outlet was constantly monitored using a mass spectrometer (Omnistar, Pfeiffer Vacuum). The recorded spectra (4 cm^{-1} resolution; 100 spectra) were converted to the Kubelka-Munk function using the OPUS software (Bruker).

UHV-FTIR Spectroscopy and XPS

The ultra-high vacuum Fourier transform infrared spectroscopy (UHV-FTIRS) and X-ray photoelectron spectroscopy (XPS) measurements were conducted with a sophisticated UHV apparatus combing a state-of-the-art FTIR spectrometer (Bruker Vertex 80v) and a multichamber UHV system (Prevac). This dedicated apparatus was built in a way that the spectrometer can be attached to the experimental chamber and measures the IR spectra through the UHV chamber. Additionally, it allows performing both IR transmission experiments on nanostructured powders and XPS measurements on samples without

removing the material from UHV, allowing both measurements without exposing it to atmosphere.[39]

The powder samples (approximately 5 mg) were pressed into an inert metal mesh (stainless steel, 150x150 wires/inch, 0.37 open area, plain weave) and then mounted on a sample holder (Prevac) specially designed for transmission FTIR measurements. After introduction of the powders into UHV (10^{-10} mbar) the surface was cleaned via heating to 700 K (427 °C), for one hour, in the presence of oxygen atmosphere (10^{-5} mbar) to get the cleaned surface or without any oxygen (10^{-10} mbar) to get the reduced surface. After cooling the sample to temperatures as low as 120 K (-153 °C) exposure to carbon monoxide (CO) was achieved using a leak-valve-based directional doser connected to a tube of 2 mm in diameter, which is terminated 3 cm from the sample surface and 50 cm from the hot-cathode ionization gauge. The XPS experiments were performed using a VG Scienta R4000 electron energy analyser at room temperature. The binding energies were calibrated using the Ce (IV) $3d_{5/2}$ line at 882.0 eV as a reference. The XPS spectra were deconvoluted using the software Casa XPS, using a Shirley background with a Gaussian-Lorentzian mix fitting function, keeping the ratios and the separation of the individual spin-orbit splitting constant.

Density functional theory calculations

Density functional theory (DFT) calculations were performed using the Vienna Ab initio Simulation Package (VASP) in connection with the Atomic Simulation Environment (ASE). All calculations used the projector augmented wave method (PAW), and the Bayesian error estimation functional with van der Waals correlations (BEEF-vdW). A plane-wave basis set with a cut-off energy of 415 eV was used. For a better description of localized Ce 4f electrons, the GGA+U method was applied, with U being 4.5 eV. The lattice constant of CeO_2 was 5.499 Å. A four layers thick unit cell with 2x2 for the (111) and the (110) surfaces, and $2\sqrt{2}x\sqrt{2}$ for the (100) surface was used for the infinite slabs. One Pd atom is adsorbed on several surface facets of (111), (110) and (100). In the case of a substituted cerium atom, a defect is created by the removal of one cerium atom on the surface facets of (110) and (111) to replace it by a Pd atom, which is here called Pd substituted. All slabs were separated by more than 15 Å of vacuum in the z direction. The Pd cluster with 10 Pd atoms was calculated on 6x6 large unit cells of CeO_2 (111) with a vacuum in z direction of 15 Å and a two layers thick slab with the bottom layer fixed. All atoms in the top two layers of the CeO_2 (111) surface as well as the Pd and all adsorbates were allowed to relax during the geometry optimizations. The Brillouin zones were sampled using a (4x5x1), (4x6x1),

and (3x6x1) Monkhorst−Pack k-point grid for the CeO_2 (111), CeO_2 (110), and CeO_2 (100) surfaces with single atoms, respectively, and a (1x1x1) Monkhorst−Pack k-point grid for the Pd_{10} cluster on CeO_2 (111). A Fermi smearing with a width of 0.1 eV was used. The convergence criterion for geometry optimizations was a maximum force of $1e^{-7}$ eV/Å. Spin polarization was considered in all calculations. Structures used for the EXAFS fitting were calculated using slightly different parameters for the plane-wave cut-off (450 eV) and U (U=5.0eV) resulting in a lattice constant of 5.519 Å. Free energies were computed using the harmonic approximation. The vibrational frequencies were calculated from the finite difference method including only the adsorbed CO. For the supported Pd_{10} cluster, the vibrational calculations were performed for all 7-10 adsorbed CO molecules simultaneously. The frequencies of adsorbed CO have been corrected by a scaling factor of 1.0085 since DFT yields vibrations for CO in the gas-phase that are slightly off from the experimental value of 2143 cm^{-1} (BEEF-vdW: 2125 cm^{-1}).

Ex situ characterization

Table S1: Overview of BET and elemental analysis results for the FSP-prepared samples.

Sample	BET surface area/ $m^2\ g^{-1}$	Noble metal loading / %
0.5% Pd/CeO_2	110	0.42
0.5% Pd/CeO_2-SF	134	0.43
1.0% Pd/CeO_2-SF	117	0.87
0.5% Pd/Al_2O_3	267	0.37
0.5% Pd/5% CeO_2-Al_2O_3	239	0.39
0.5% Pd/10% CeO_2-Al_2O_3	216	0.37

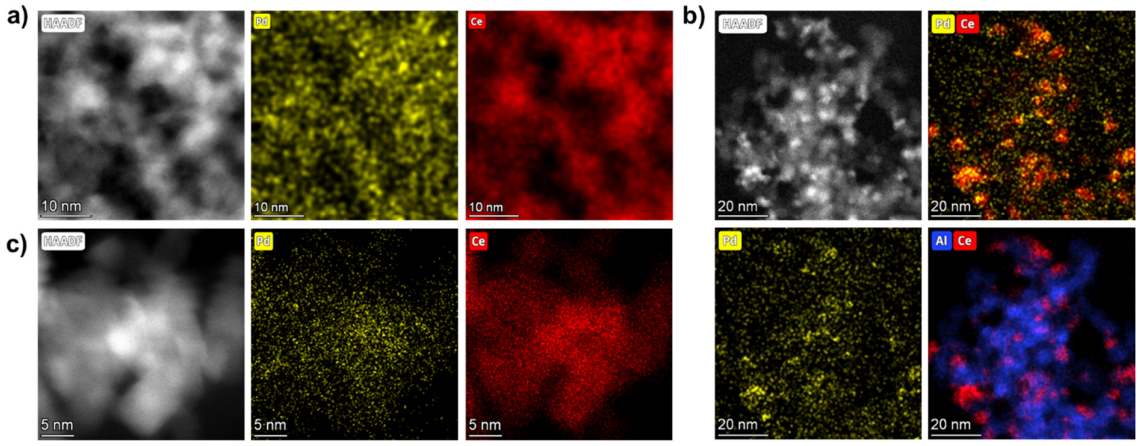

Figure S1: HAADF-STEM images with corresponding EDXS mappings for 0.5% Pd/CeO_2-SF (a), 0.5% Pd/10% CeO_2-Al_2O_3 (b) and 1.0% Pd/CeO_2-SF (c).

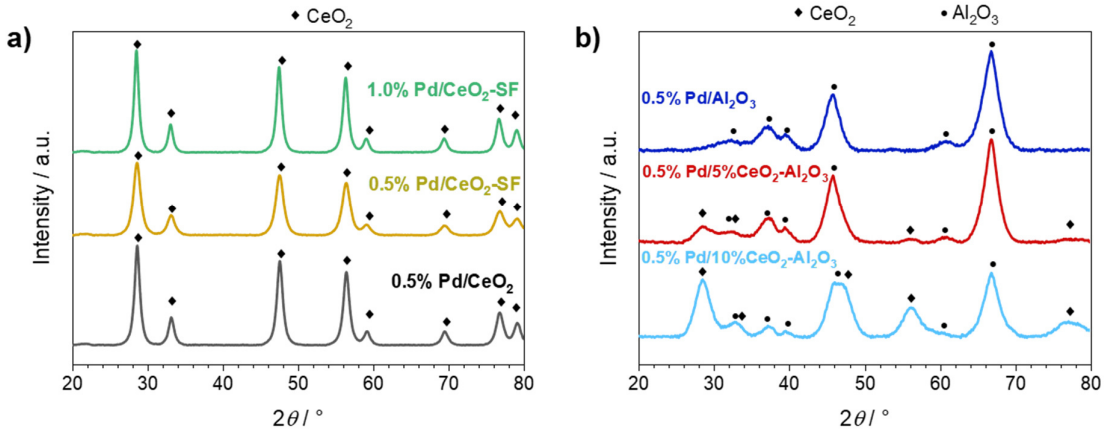

Figure S2: XRD patterns of the FSP-synthesized catalysts. The assignment of the XRD reflections was performed based on the data from crystallographic database (ICSD (CeO_2): 24887, ICSD (Al_2O_3): 249140).

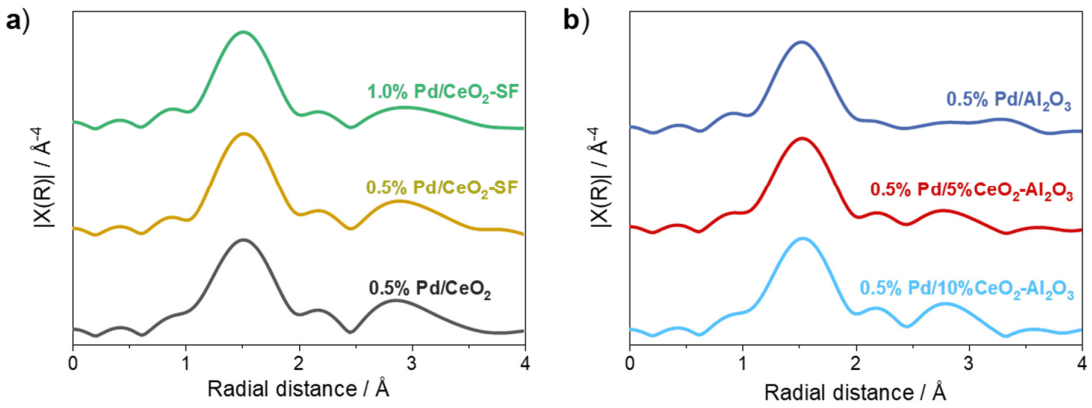

Figure S3: *Ex situ* FT-EXAFS data in R-space of the FSP-prepared catalysts.

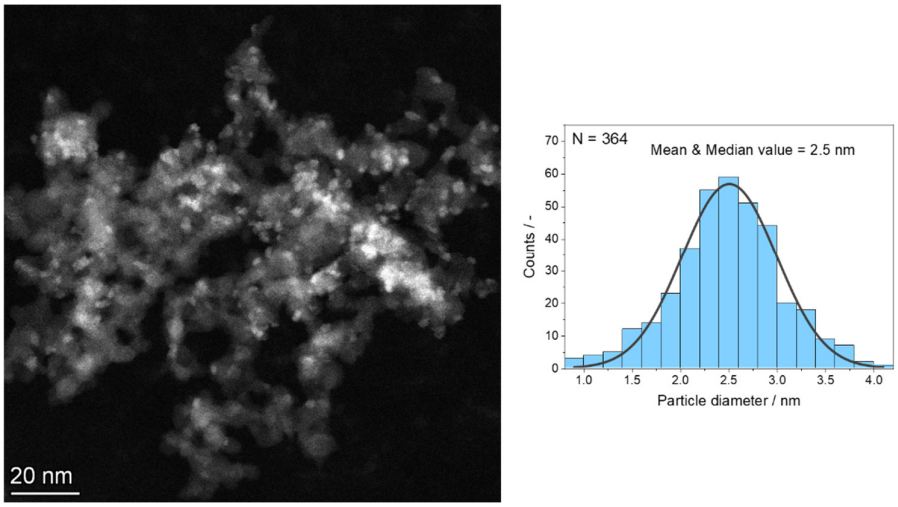

Figure S4: HAADF-STEM image (left) and particle size distribution of CeO_2 nano-islands (diameter of the islands, right) in the 0.5% Pd/5% CeO_2-Al_2O_3 catalyst. For the estimation of the particle diameter, a spherical shape of the particles was assumed. This is valid for the major fraction (>90 %) of the counted CeO_2 nano-islands. The remaining CeO_2 nanoparticles (<10 %) have an ellipsoidal shape. For these particles, an effective particle diameter was calculated as $\sqrt{d_1 \cdot d_2}$ by assuming that the area of an ellipse is equal to the area of a circle with an effective diameter. The average particle diameter was determined *via* fitting the particle size distribution with a Gauss function (FHWM = 1.2 nm).

Estimation of maximum Pd cluster size on each CeO_2 nano-island

The volume of each CeO_2 nano-island was calculated assuming a spherical shape and an average particle size of 2.5 nm, according to the results of the particle size distribution analysis shown in Figure S4.

$$V = \frac{4}{3}\pi r^3$$

From the obtained volume, the mass of each spherical CeO_2 particle was determined with the following formula, with density of CeO_2 (**ρ)** of 7.22 g cm^{-3}:

$$m = \frac{V}{\rho}$$

In the next step, the mass of a Pd cluster on each CeO_2 nano-island was estimated based on the Pd:CeO_2 weight ratio of 1:10 for the 0.5% Pd/5% CeO_2-Al_2O_3 catalyst. It should be noted, that the Pd:CeO_2 ratio of 1:10 corresponds to a molar ratio of 1:6.

Using a molar mass of Pd (M = 106.42 g mol^{-1}) and Avogadro number (N_A = $6.022 \cdot 10^{23}$ mol^{-1}), the number of Pd atoms on one CeO_2 island was calculated from the mass of a Pd cluster (m_{Pd}) as follows:

$$N = \frac{m_{Pd} N_A}{M}$$

The observed values are summarized in Table S2.

Table S2: Estimation of the maximum size of a Pd cluster on each CeO_2 nano-island.

Average CeO_2 particle diameter / nm	Average volume of one CeO_2 island / nm^3	Average Mass of one CeO_2 island / 10^{-20} g	Pd:CeO_2 weight ratio	Average mass of Pd on one CeO_2 island / 10^{-21} g	Average number of Pd atoms on one CeO_2 island
2.5	8.2	5.9	1:10	5.9	33

EXAFS fitting

Table S3: Restrictions of the fitting parameters used for EXAFS analysis.

Parameter	Restriction
Amplitude reduction factor	0.75 determined by fitting of Pd foil with Pd model (ICSD 64914)
Coordination number	Fit with one structure: $0 < CN < 1$, multiplied by the path degeneracy Fit with two structures (substituted Pd^{2+}/CeO_2 and PdO): Substituted Pd^{2+}/CeO_2: $0 < CN_1 < 1$, multiplied by the path degeneracy Bulk PdO: $CN_2 = (1-CN_1)$
Mean squared displacement	$0.001 < \delta^2 < 0.03$ for PdO structure $0.001 < \delta^2 < 0.01$ for DFT-calculated models

Table S4: Paths included in the fitting model used for EXAFS analysis.

Structure	Included path (degeneracy)	Effective path length / Å
Bulk PdO (ICSD 24692)	O (4)	2.018
	Pd (4)	3.030
	Pd (8)	3.419
(110) adsorbed Pd^{2+}/CeO_2	O (2)	1.957
	O (1)	2.087
	Ce (1)	3.122
	Ce (1)	3.349
	Ce (1)	3.493
(110) substituted Pd^{2+}/CeO_2	O (3)	2.018
	O (1)	2.038
	Ce (1)	3.059
	Ce (2)	3.138
	Ce (1)	3.253
(110) substituted Pd^{4+}/CeO_2	O (4)	2.014
	Ce (1)	2.920
	Ce (2)	3.151
	Ce (1)	3.272
(111) adsorbed Pd^{2+}/CeO_2	O (1)	1.800
	O (1)	1.992
	O (1)	2.919
	O (1)	2.953
	Ce (2)	3.380
(111) substituted Pd^{2+}/CeO_2	O (3)	2.018
	O (1)	2.045
	Ce (1)	3.131
	Ce (1)	3.163
	Ce (1)	3.197
	Ce (1)	3.301
(111) substituted Pd^{4+}/CeO_2	O (1)	1.890
	O (3)	1.984
	Ce (4)	3.325

Table S5: Calculated Bader charges.

Structure	Bader charge
Bulk PdO_2	8.40
Bulk PdO	9.05
(110) substituted Pd^{4+}/CeO_2	8.85
110 PdO_2-sub [a]	9.08

[a)] This structure is more stable by 0.65 eV than (110) substituted Pd^{4+}/CeO_2 as it reconstructs to a more defined Pd^{2+} state as also evident from the Bader charge analysis. Formally, this can be seen as a substituted Pd^{2+} at a CeO_2 surface with an extra O^* adsorbed, structure shown in Figure S8b. This structure is also used for EXAFS analysis (see Figure 1).

Table S6: Results from the EXAFS data analysis of Pd/CeO_2 using one structural model for EXAFS fitting. In case of a strong shift of the included path (|ΔR| > 0.07 Å), the ΔR fitting parameter is marked bold.

Structure	**R factor / -**	**Included path (degeneracy)**	**Parameter**	**Dependency /-**
Bulk PdO (ICSD 24692)	0.029	O (4)	CN = 0.99 ± 0.08 ΔE_0 = 3.43 ± 1.53 ΔR = -0.021 ± 0.013 δ^2 = 0.00099 ± 0.0001	CN_1 E_1 ΔR_1 $\delta^2{}_1$
		Pd (4)	CN = 0.99 ± 0.08 ΔE_0 = 3.43 ± 1.53 **ΔR = -0.085 ± 0.023** δ^2 = 0.014 ± 0.0026	CN_1 E_1 ΔR_2 $\delta^2{}_2$
		Pd (8)	CN = 0.99 ± 0.08 ΔE_0 = 3.43 ± 1.53 **ΔR = -0.085 ± 0.023** δ^2 = 0.014 ± 0.0026	CN_1 E_1 ΔR_2 $\delta^2{}_2$
(110) adsorbed Pd^{2+}/CeO_2 (110 PdO-add)	0.261	O (2)	CN = 1.00 ± 0.03 ΔE_0 = 2.63 ± 7.05 ΔR = -0.022 ± 0.075 δ^2 = 0.00098 ± 0.0003	CN_1 E_1 ΔR_1 $\delta^2{}_1$
		O (1)	CN = 1.00 ± 0.03 ΔE_0 = 2.63 ± 7.05 ΔR = -0.022 ± 0.075 δ^2 = 0.00098 ± 0.0003	CN_1 E_1 ΔR_1 $\delta^2{}_1$
		Ce (1)	CN = 1.00 ± 0.03 ΔE_0 = 2.63 ± 7.05 **ΔR = 0.097 ± 0.117** δ^2 = 0.00099 ± 0.0003	CN_1 E_1 ΔR_2 $\delta^2{}_2$
		Ce (1)	CN = 1.00 ± 0.03 ΔE_0 = 2.63 ± 7.05 **ΔR = 0.097 ± 0.117** δ^2 = 0.00099 ± 0.0003	CN_1 E_1 ΔR_2 $\delta^2{}_2$
		Ce (1)	CN = 1.00 ± 0.03 ΔE_0 = 2.63 ± 7.05 **ΔR = 0.097 ± 0.117** δ^2 = 0.00099 ± 0.0003	CN_1 E_1 ΔR_2 $\delta^2{}_2$
(110) substituted Pd^{2+}/CeO_2 (110 PdO-sub)	0.036	O (3)	CN = 0.99 ± 0.09 ΔE_0 = 0.24 ± 1.80 ΔR = -0.025 ± 0.016 δ^2 = 0.00099 ± 0.0001	CN_1 E_1 ΔR_1 $\delta^2{}_1$
		O (1)	CN = 0.99 ± 0.09 ΔE_0 = 0.24 ± 1.80 ΔR = -0.025 ± 0.016	CN_1 E_1 ΔR_1

			δ^2 = 0.00099 ± 0.0001	δ^2_1
		Ce (1)	CN = 0.99 ± 0.09	CN_1
			ΔE_0 = 0.24 ± 1.80	E_1
			ΔR = 0.052 ± 0.029	ΔR_2
			δ^2 = 0.0019 ± 0.0031	δ^2_2
		Ce (2)	CN = 0.99 ± 0.09	CN_1
			ΔE_0 = 0.24 ± 1.80	E_1
			ΔR = 0.052 ± 0.029	ΔR_2
			δ^2 = 0.0019 ± 0.0031	δ^2_2
		Ce (1)	CN = 0.99 ± 0.09	CN_1
			ΔE_0 = 0.24 ± 1.80	E_1
			ΔR = 0.052 ± 0.029	ΔR_2
			δ^2 = 0.0019 ± 0.0031	δ^2_2
(110) substituted Pd^{4+}/CeO_2 (110 PdO_2-sub)	0.031	O (4)	CN = 1.00 ± 0.01	CN_1
			ΔE_0 = -0.44 ± 1.79	E_1
			ΔR = -0.024 ± 0.015	ΔR_1
			δ^2 = 0.00099 ± 0.00096	δ^2_1
		Ce (1)	CN = 1.00 ± 0.01	CN_1
			ΔE_0 = -0.44 ± 1.79	E_1
			ΔR = -0.029 ± 0.023	ΔR_2
			δ^2 = 0.0013 ± 0.0022	δ^2_2
		Ce (2)	CN = 1.00 ± 0.01	CN_1
			ΔE_0 = -0.44 ± 1.79	E_1
			ΔR = -0.029 ± 0.023	ΔR_2
			δ^2 = 0.0013 ± 0.0022	δ^2_2
		Ce (1)	CN = 1.00 ± 0.01	CN_1
			ΔE_0 = -0.44 ± 1.79	E_1
			ΔR = -0.029 ± 0.023	ΔR_2
			δ^2 = 0.0013 ± 0.0022	δ^2_2
(111) adsorbed Pd^{2+}/CeO_2 (111 PdO-add)	0.59	O (1)	CN = 1.00 ± 0.06	CN_1
			ΔE_0 = -0.34 ± 18.9	E_1
			ΔR = 0.115 ± 0.306	ΔR_1
			δ^2 = 0.00098 ± 0.00056	δ^2_1
		O (1)	CN = 1.00 ± 0.06	CN_1
			ΔE_0 = -0.34 ± 18.9	E_1
			ΔR = 0.115 ± 0.306	ΔR_1
			δ^2 = 0.00098 ± 0.00056	δ^2_1
		O (1)	CN = 1.00 ± 0.06	CN_1
			ΔE_0 = -0.34 ± 18.9	E_1
			ΔR = -0.243 ± 0.344	ΔR_2
			δ^2 = 0.003 ± 0.00056	δ^2_2

		O (1)	CN = 1.00 ± 0.06 ΔE_0 = -0.34 ± 18.9 **ΔR = -0.243 ± 0.344** δ^2 = 0.003 ± 0.00056	CN_1 E_1 ΔR_2 $\delta^2{}_2$
		Ce (2)	CN = 1.00 ± 0.06 ΔE_0 = -0.34 ± 18.9 **ΔR = -0.213 ± 0.18** δ^2 = 0.0026 ± 0.0155	CN_1 E_1 ΔR_3 $\delta^2{}_3$
(111) substituted Pd^{2+}/CeO_2 (111 PdO-sub)	0.038	O (3)	CN = 0.98 ± 0.098 ΔE_0 = 0.41 ± 1.84 ΔR = -0.0267 ± 0.0169 δ^2 = 0.00099 ± 0.0001	CN_1 E_1 ΔR_1 $\delta^2{}_1$
		O (1)	CN = 0.98 ± 0.098 ΔE_0 = 0.41 ± 1.84 ΔR = -0.0267 ± 0.0169 δ^2 = 0.00099 ± 0.0001	CN_1 E_1 ΔR_1 $\delta^2{}_1$
		Ce (1)	CN = 0.98 ± 0.098 ΔE_0 = 0.41 ± 1.84 ΔR = 0.006 ± 0.029 δ^2 = 0.0026 ± 0.0031	CN_1 E_1 ΔR_2 $\delta^2{}_2$
		Ce (1)	CN = 0.98 ± 0.098 ΔE_0 = 0.41 ± 1.84 ΔR = 0.006 ± 0.029 δ^2 = 0.0026 ± 0.0031	CN_1 E_1 ΔR_2 $\delta^2{}_2$
		Ce (1)	CN = 0.98 ± 0.098 ΔE_0 = 0.41 ± 1.84 ΔR = 0.006 ± 0.029 δ^2 = 0.0026 ± 0.0031	CN_1 E_1 ΔR_2 $\delta^2{}_2$
		Ce (1)	CN = 0.98 ± 0.098 ΔE_0 = 0.41 ± 1.84 ΔR = 0.006 ± 0.029 δ^2 = 0.0026 ± 0.0031	CN_1 E_1 ΔR_2 $\delta^2{}_2$
(111) substituted Pd^{4+}/CeO_2 (111 PdO_2-sub)	0.063	O (1)	CN = 1.00 ± 0.015 ΔE_0 = -0.15 ± 2.44 ΔR = 0.0339 ± 0.0234 δ^2 = 0.00098 ± 0.0001	CN_1 E_1 ΔR_1 $\delta^2{}_1$
		O (3)	CN = 1.00 ± 0.015 ΔE_0 = -0.15 ± 2.44 ΔR = 0.0339 ± 0.0234 δ^2 = 0.00098 ± 0.0001	CN_1 E_1 ΔR_1 $\delta^2{}_1$
		Ce (4)	CN = 1.00 ± 0.015 ΔE_0 = -0.15 ± 2.44 **ΔR = -0.142 ± 0.0384** δ^2 = 0.0071 ± 0.0038	CN_1 E_1 ΔR_2 $\delta^2{}_2$

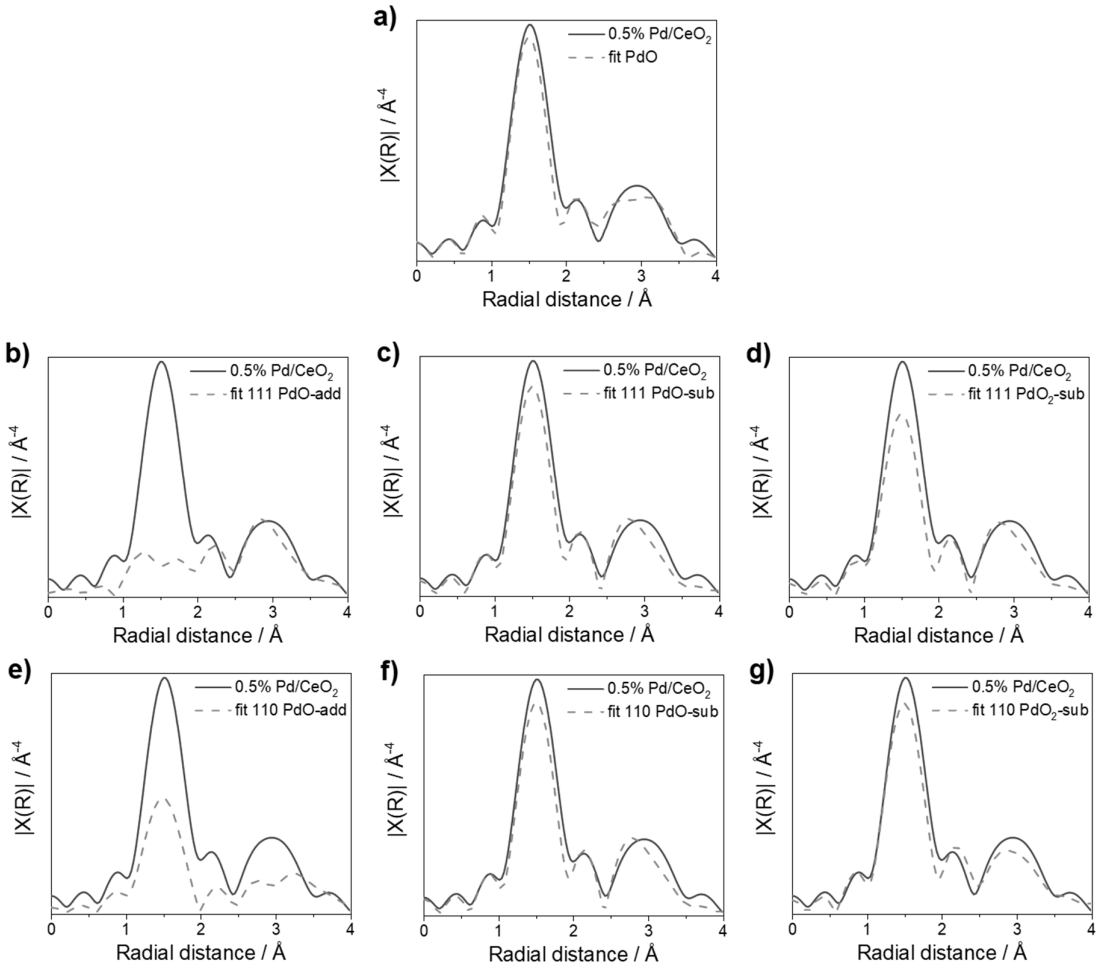

Figure S5: FT-EXAFS data at the Pd K-edge with results from the EXAFS data analysis of 0.5% Pd/CeO_2 (experimental data: solid lines; fit: dashed lines) using one structural model for EXAFS fitting.

Table S7: Results from the EXAFS data analysis of Pd/CeO_2 using combination of two structural models (PdO and Pd located in four-fold hollow site position) for EXAFS fitting. In case of a strong shift of the included path ($|\Delta R| > 0.07$ Å), the ΔR fitting parameter is marked bold.

Structure	R factor / -	Included path (degeneracy)	Parameter	Dependency / -
Bulk PdO + (110) substituted Pd^{2+}/CeO_2	0.018	O (4)	CN = 0.58 ± 0.34	$1\text{-}CN_1$
			ΔE_0 = 1.99 ± 2.23	E_1
			ΔR = -0.023 ± 0.015	ΔR_1
			δ^2 = 0.00099 ± 0.0001	δ^2_1
		Pd (4)	CN = 0.58 ± 0.34	$1\text{-}CN_1$
			ΔE_0 = 1.99 ± 2.23	E_1
			ΔR = -0.075 ± 0.038	ΔR_2
			δ^2 = 0.012 ± 0.0007	δ^2_2
		Pd (8)	CN = 0.58 ± 0.34	$1\text{-}CN_1$
			ΔE_0 = 1.99 ± 2.23	E_1
			ΔR = -0.075 ± 0.038	ΔR_2
			δ^2 = 0.012 ± 0.0007	δ^2_2
		O (3)	CN = 0.42 ± 0.34	CN_1
			ΔE_0 = 1.99 ± 2.23	E_1
			ΔR = -0.023 ± 0.015	ΔR_1
			δ^2 = 0.0001 ± 0.0001	δ^2_1
		O (1)	CN = 0.42 ± 0.34	CN_1
			ΔE_0 = 1.99 ± 2.23	E_1
			ΔR = -0.023 ± 0.015	ΔR_1
			δ^2 = 0.00099 ± 0.0001	δ^2_1
		Ce (1)	CN = 0.42 ± 0.34	CN_1
			ΔE_0 = 1.99 ± 2.23	E_1
			ΔR = 0.028 ± 0.090	ΔR_3
			δ^2 = 0.00099 ± 0.0006	δ^2_3
		Ce (2)	CN = 0.42 ± 0.34	CN_1
			ΔE_0 = 1.99 ± 2.23	E_1
			ΔR = 0.028 ± 0.090	ΔR_3
			δ^2 = 0.00099 ± 0.0006	δ^2_3
		Ce (1)	CN = 0.42 ± 0.34	CN_1
			ΔE_0 = 1.99 ± 2.23	E_1
			ΔR = 0.028 ± 0.090	ΔR_3
			δ^2 = 0.00099 ± 0.0006	δ^2_3
Bulk PdO + (111) substituted Pd^{2+}/CeO_2	0.018	O (4)	CN = 0.60 ± 0.34	$1\text{-}CN_1$
			ΔE_0 = 2.09 ± 2.18	E_1
			ΔR = -0.024 ± 0.015	ΔR_1
			δ^2 = 0.00099 ± 0.0001	δ^2_1

		Pd (4)	CN = 0.60 ± 0.34 ΔE_0 = 2.09 ± 2.18 **ΔR = -0.073 ± 0.042** δ^2 = 0.0012 ± 0.0074	$1\text{-}CN_1$ E_1 ΔR_2 δ^2_2
		Pd (8)	CN = 0.60 ± 0.34 ΔE_0 = 2.09 ± 2.18 **ΔR = -0.073 ± 0.042** δ^2 = 0.0012 ± 0.0074	$1\text{-}CN_1$ E_1 ΔR_2 δ^2_2
		O (3)	CN = 0.40 ± 0.34 ΔE_0 = 2.09 ± 2.18 ΔR = -0.024 ± 0.015 δ^2 = 0.00099 ± 0.0001	CN_1 E_1 ΔR_1 δ^2_1
		O (1)	CN = 0.40 ± 0.34 ΔE_0 = 2.09 ± 2.18 ΔR = -0.024 ± 0.015 δ^2 = 0.00099 ± 0.0001	CN_1 E_1 ΔR_1 δ^2_1
		Ce (1)	CN = 0.40 ± 0.34 ΔE_0 = 2.09 ± 2.18 ΔR = -0.017 ± 0.090 δ^2 = 0.00099 ± 0.0006	CN_1 E_1 ΔR_3 δ^2_3
		Ce (1)	CN = 0.40 ± 0.34 ΔE_0 = 2.09 ± 2.18 ΔR = -0.017 ± 0.090 δ^2 = 0.00099 ± 0.0006	CN_1 E_1 ΔR_3 δ^2_3
		Ce (1)	CN = 0.40 ± 0.34 ΔE_0 = 2.09 ± 2.18 ΔR = -0.017 ± 0.090 δ^2 = 0.00099 ± 0.0006	CN_1 E_1 ΔR_3 δ^2_3
		Ce (1)	CN = 0.40 ± 0.34 ΔE_0 = 2.09 ± 2.18 ΔR = -0.017 ± 0.090 δ^2 = 0.00099 ± 0.0006	CN_1 E_1 ΔR_3 δ^2_3

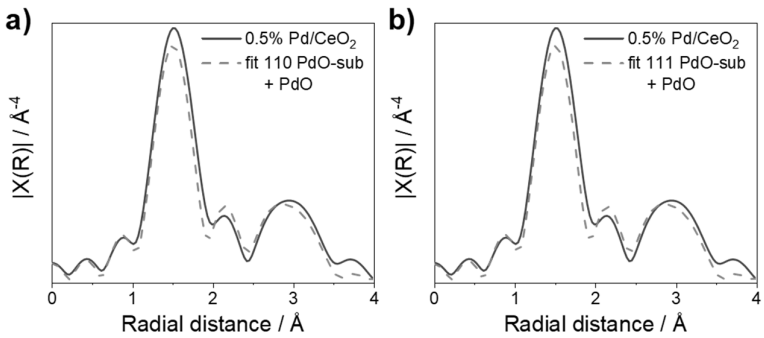

Figure S6: FT-EXAFS data at the Pd K-edge with results from the EXAFS data analysis of 0.5% Pd/CeO_2 (experimental data: solid lines; fit: dashed lines) using combination of two structural models for EXAFS fitting (substituted Pd^{2+}/CeO_2 and bulk PdO).

Table S8: Results from the EXAFS data analysis of 0.5% Pd/5% CeO_2-Al_2O_3 using one structural model for EXAFS fitting. In case of a strong shift of the included path (|ΔR| > 0.07 Å), the ΔR fitting parameter is marked bold.

Structure	R factor / -	Included path (degeneracy)	Parameter	Dependency /-
Bulk PdO	0.029	O (4)	CN = 0.96 ± 0.07	CN_1
			ΔE_0 = 2.46 ± 1.46	E_1
			ΔR = -0.021 ± 0.013	ΔR_1
			δ^2 = 0.00099 ± 0.00016	δ^2_1
		Pd (4)	CN = 0.96 ± 0.07	CN_1
			ΔE_0 = 2.46 ± 1.46	E_1
			ΔR = -0.106 ± 0.036	ΔR_2
			δ^2 = 0.019 ± 0.0044	δ^2_2
		Pd (8)	CN = 0.96 ± 0.07	CN_1
			ΔE_0 = 2.46 ± 1.46	E_1
			ΔR = -0.106 ± 0.036	ΔR_2
			δ^2 = 0.019 ± 0.0044	δ^2_2
(110) adsorbed Pd^{2+}/CeO_2	0.218	O (2)	CN = 1.00 ± 0.05	CN_1
			ΔE_0 = 1.13 ±6.19	E_1
			ΔR = 0.017 ± 0.065	ΔR_1
			δ^2 = 0.00093 ± 0.0005	δ^2_1
		O (1)	CN = 1.00 ± 0.05	CN_1
			ΔE_0 = 1.13 ±6.19	E_1
			ΔR = 0.017 ± 0.065	ΔR_1
			δ^2 = 0.00093 ± 0.0005	δ^2_1
		Ce (1)	CN = 1.00 ± 0.05	CN_1
			ΔE_0 = 1.13 ±6.19	E_1
			ΔR = 0.058 ± 0.121	ΔR_2
			δ^2 = 0.00271 ± 0.0124	δ^2_2
		Ce (1)	CN = 1.00 ± 0.05	CN_1
			ΔE_0 = 1.13 ±6.19	E_1
			ΔR = 0.058 ± 0.121	ΔR_2
			δ^2 = 0.00271 ± 0.0124	δ^2_2
		Ce (1)	CN = 1.00 ± 0.05	CN_1
			ΔE_0 = 1.13 ±6.19	E_1
			ΔR = 0.058 ± 0.121	ΔR_2
			δ^2 = 0.00271 ± 0.0124	δ^2_2
(110) substituted Pd^{2+}/CeO_2	0.051	O (3)	CN = 0.95 ± 0.10	CN_1
			ΔE_0 = -0.84 ± 2.26	E_1
			ΔR = -0.025 ± 0.0189	ΔR_1
			δ^2 = 0.00099 ± 0.0002	δ^2_1
		O (1)	CN = 0.95 ± 0.10	CN_1
			ΔE_0 = -0.84 ± 2.26	E_1
			ΔR = -0.025 ± 0.0189	ΔR_1

			$\delta^2 = 0.00099 \pm 0.0002$	δ^2_1
		Ce (1)	CN = 0.95 ± 0.10	CN_1
			$\Delta E_0 = -0.84 \pm 2.27$	E_1
			$\Delta R = 0.112 \pm 0.064$	ΔR_2
			$\delta^2 = 0.01 \pm 0.0002$	δ^2_2
		Ce (2)	CN = 0.95 ± 0.10	CN_1
			$\Delta E_0 = -0.84 \pm 2.27$	E_1
			$\Delta R = 0.112 \pm 0.064$	ΔR_2
			$\delta^2 = 0.01 \pm 0.0002$	δ^2_2
		Ce (1)	CN = 0.95 ± 0.10	CN_1
			$\Delta E_0 = -0.84 \pm 2.27$	E_1
			$\Delta R = 0.112 \pm 0.064$	ΔR_2
			$\delta^2 = 0.01 \pm 0.0002$	δ^2_2
(110) substituted Pd^{4+}/CeO_2	0.022	O (4)	CN = 0.99 ± 0.07	CN_1
			$\Delta E_0 = -0.96 \pm 1.62$	E_1
			$\Delta R = -0.021 \pm 0.013$	ΔR_1
			$\delta^2 = 0.00099 \pm 0.00015$	δ^2_1
		Ce (1)	CN = 0.99 ± 0.07	CN_1
			$\Delta E_0 = -0.96 \pm 1.62$	E_1
			$\Delta R = -0.058 \pm 0.029$	ΔR_2
			$\delta^2 = 0.0048 \pm 0.0034$	δ^2_2
		Ce (2)	CN = 0.99 ± 0.07	CN_1
			$\Delta E_0 = -0.96 \pm 1.62$	E_1
			$\Delta R = -0.058 \pm 0.029$	ΔR_2
			$\delta^2 = 0.0048 \pm 0.0034$	δ^2_2
		Ce (1)	CN = 0.99 ± 0.07	CN_1
			$\Delta E_0 = -0.96 \pm 1.62$	E_1
			$\Delta R = -0.058 \pm 0.029$	ΔR_2
			$\delta^2 = 0.0048 \pm 0.0034$	δ^2_2
(111) substituted Pd^{2+}/CeO_2	0.051	O (3)	CN = 0.95 ± 0.11	CN_1
			$\Delta E_0 = -0.66 \pm 2.25$	E_1
			$\Delta R = -0.027 \pm 0.019$	ΔR_1
			$\delta^2 = 0.00098 \pm 0.0002$	δ^2_1
		O (1)	CN = 0.95 ± 0.11	CN_1
			$\Delta E_0 = -0.66 \pm 2.25$	E_1
			$\Delta R = -0.027 \pm 0.019$	ΔR_1
			$\delta^2 = 0.00098 \pm 0.0002$	δ^2_1
		Ce (1)	CN = 0.95 ± 0.11	CN_1
			$\Delta E_0 = -0.66 \pm 2.25$	E_1
			$\Delta R = -0.036 \pm 0.061$	ΔR_2
			$\delta^2 = 0.01 \pm 0.0002$	δ^2_2

		Ce (1)	CN = 0.95 ± 0.11	CN_1
			ΔE_0 = -0.66 ± 2.25	E_1
			ΔR = -0.036 ± 0.061	ΔR_2
			δ^2 = 0.01± 0.0002	δ^2_2
		Ce (1)	CN = 0.95 ± 0.11	CN_1
			ΔE_0 = -0.66 ± 2.25	E_1
			ΔR = -0.036 ± 0.061	ΔR_2
			δ^2 = 0.01± 0.0002	δ^2_2
		Ce (1)	CN = 0.95 ± 0.11	CN_1
			ΔE_0 = -0.66 ± 2.25	E_1
			ΔR = -0.036 ± 0.061	ΔR_2
			δ^2 = 0.01± 0.0002	δ^2_2

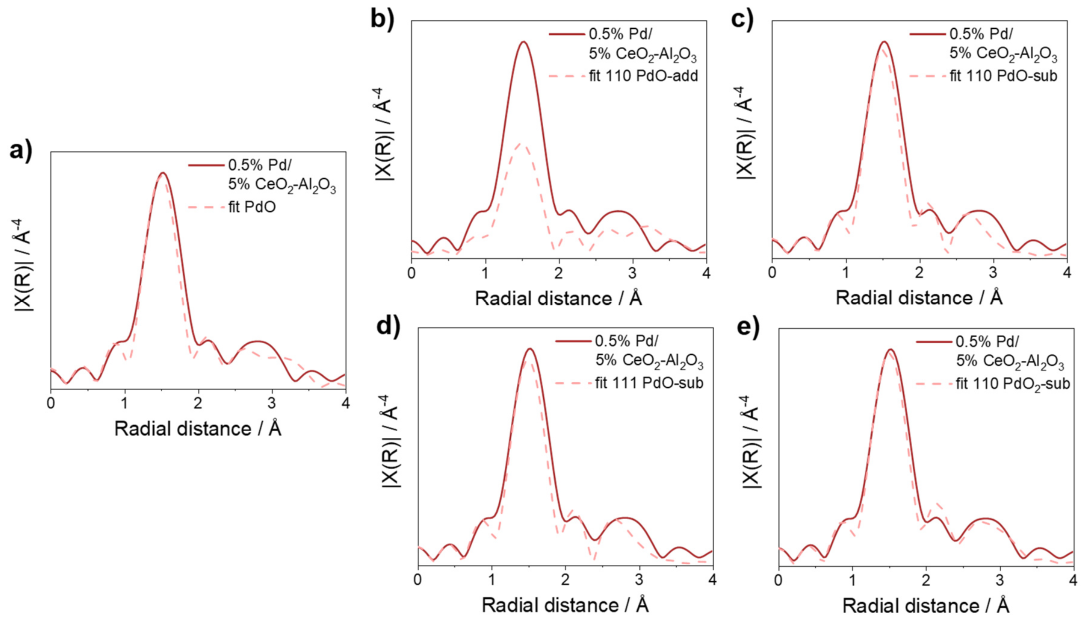

Figure S7: FT-EXAFS data at the Pd K-edge with results from the EXAFS data analysis of 0.5% Pd/5% CeO_2-Al_2O_3 (experimental data: solid lines; fit: dashed lines) using one structural model for EXAFS fitting.

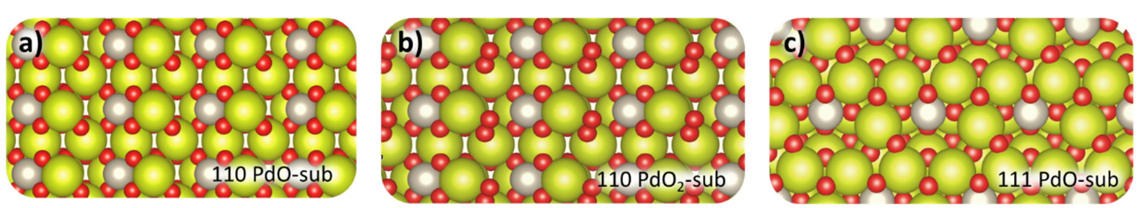

Figure S8: Structures showing good agreement with experimental EXAFS data for 0.5% Pd/CeO_2 and 0.5% Pd/5% CeO_2-Al_2O_3.

Table S9: Results from the EXAFS data analysis of 0.5% Pd/Al_2O_3 using one structural model for EXAFS fitting.

Structure	R factor / -	Included path (degeneracy)	Parameter	Dependency /-
Bulk PdO	0.031	O (4)	CN = 0.94 ± 0.07	CN_1
			ΔE_0 = 2.49 ± 1.60	E_1
			ΔR = -0.011 ± 0.014	ΔR_1
			δ^2 = 0.00099 ± 0.0002	δ^2_1
		Pd (4)	CN = 0.94 ± 0.07	CN_1
			ΔE_0 = 2.49 ± 1.60	E_1
			ΔR = 0.008 ± 0.037	ΔR_2
			δ^2 = 0.0178 ± 0.0045	δ^2_2
		Pd (8)	CN = 0.94 ± 0.07	CN_1
			ΔE_0 = 2.49 ± 1.60	E_1
			ΔR = 0.008 ± 0.037	ΔR_2
			δ^2 = 0.0178 ± 0.0045	δ^2_2

Catalytic activity data

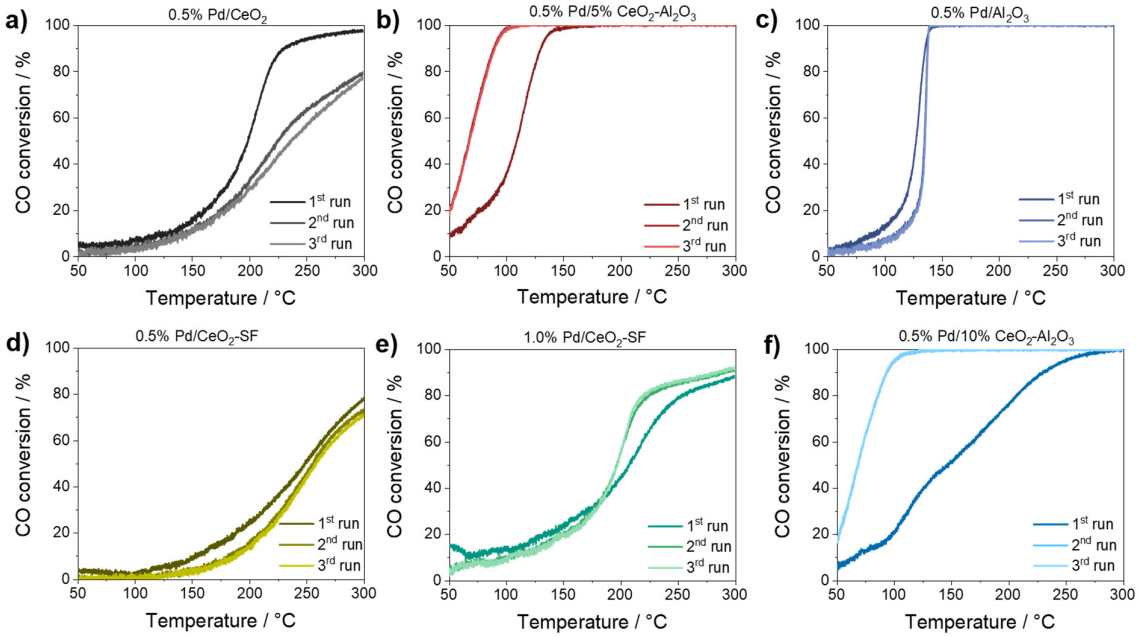

Figure S9: Catalytic activity in terms of CO conversion during three consecutive catalytic cycles in 1000 ppm CO/8% O_2/N_2 of 0.5% Pd/CeO_2 (a), 0.5% $Pd/5\%\ CeO_2$-Al_2O_3 (b), 0.5% Pd/Al_2O_3 (c), 0.5% Pd/CeO_2-SF (d); 1.0% Pd/CeO_2-SF (e), and 0.5% $Pd/10\%\ CeO_2$-Al_2O_3 (f).

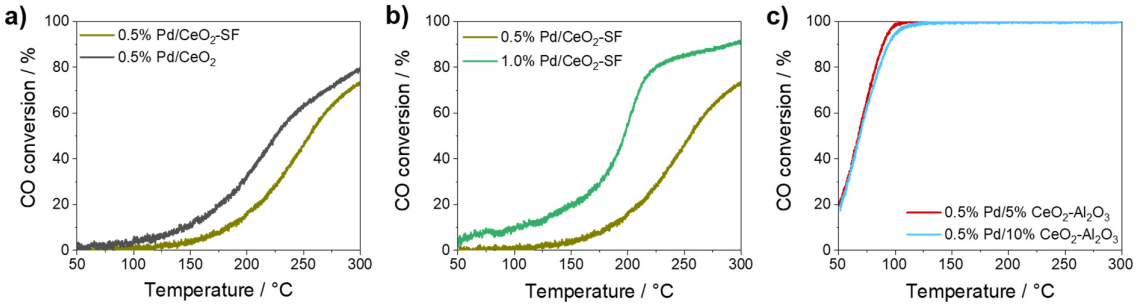

Figure S10: Catalytic activity in terms of CO conversion during the second catalytic cycle in 1000 ppm CO/8% O_2/N_2 of 0.5% Pd/CeO_2 (grey) in comparison to 0.5% Pd/CeO_2-SF (olive) (a), 0.5% Pd/CeO_2-SF (olive) in comparison to 1.0% Pd/CeO_2-SF (green) (b), and 0.5% $Pd/5\%\ CeO_2$-Al_2O_3 (red) in comparison to 0.5% $Pd/10\%\ CeO_2$-Al_2O_3 (light blue) (c).

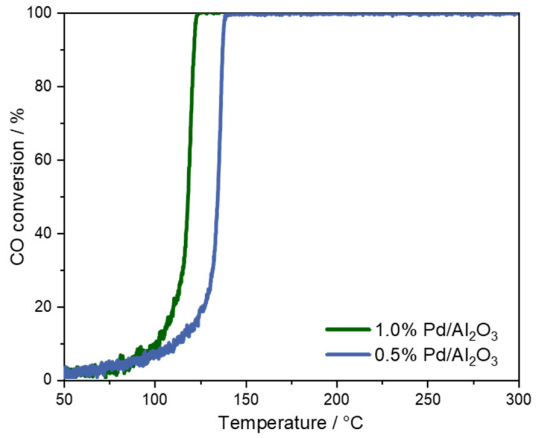

Figure S11: Catalytic activity in terms of CO conversion during the second catalytic cycle in 1000 ppm CO/8% O_2/N_2 of 0.5% Pd/Al_2O_3, prepared by double-nozzle flame spray pyrolysis (blue), in comparison to a standard 1.0% Pd/Al_2O_3 catalyst synthesized via incipient wetness impregnation (green). The catalyst amount was normalized to the noble metal loading.

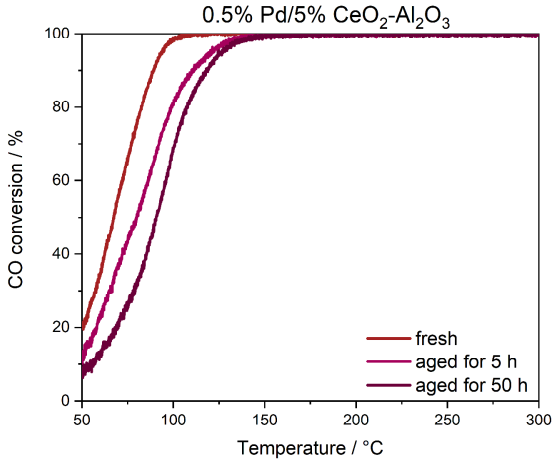

Figure S12: Catalytic activity In terms of CO conversion during the second catalytic cycle in 1000 ppm CO/8% O_2/N_2 of 0.5% Pd/5% CeO_2-Al_2O_3 in a fresh state (red), after aging at 800 °C for 5 h (violet) and 50 h (dark violet).

DFT-calculated structures and corresponding CO vibrational frequencies

Table S10: Calculated CO vibrational frequencies for CO adsorbed on Pd located on (111) and (110) ceria lattice using a scaling factor of 1.0085.

Structure	**Wavenumber / cm^{-1}**
CeO_2 (111) PdO_2	2137[a]
CeO_2 (111) PdO	2105[a]
CeO_2 (111) Pd	2057[a]
CeO_2 (110) PdO_2	2117[b]
CeO_2 (110) PdO	2095
CeO_2 (110) Pd	2023
CeO_2 (100) PdO_2	-
CeO_2 (100) PdO	2096[a]
CeO_2 (100) Pd	2068[a]

[a] from ref. [45] [b] configuration slightly changed through CO adsorption.

Table S11: Calculated CO vibrational frequencies for one CO molecule adsorbed on different Pd sites in subnanometer clusters containing 10 Pd atoms on CeO_2(111).

Structure	**Pd_{10}, flower**
CO bonding	**Wavenumber / cm^{-1}**
Ontop	2034
Bridged	1885
Hollow	1795

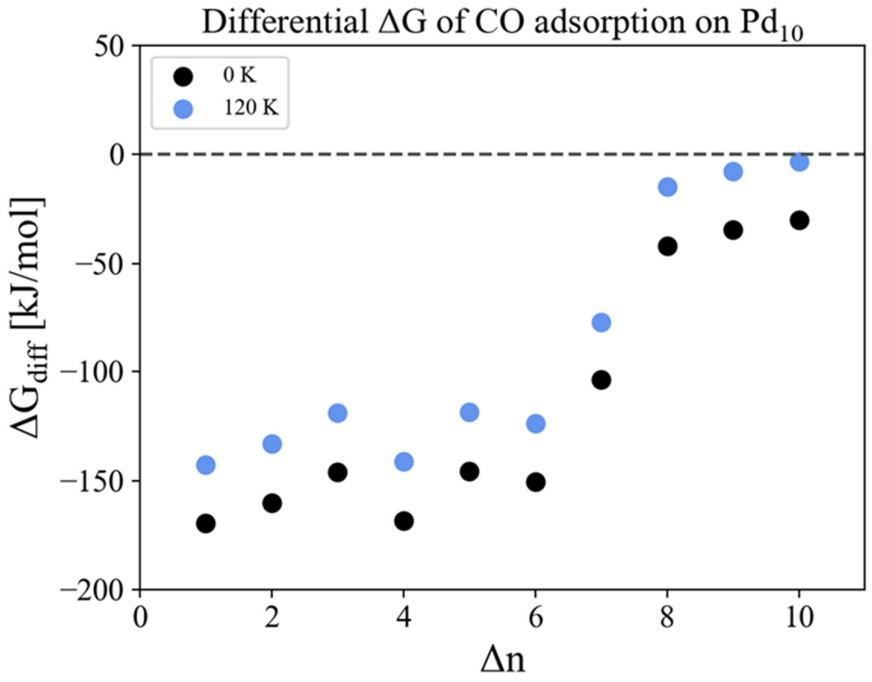

Figure S13: Calculated differential free energy of CO adsorption as a function of the number of CO molecules adsorbed on the Pd_{10}/CeO_2 (111) cluster at -153 and -273 °C (120 and 0 K) and 1 bar of CO. The Pd_{10} cluster with 7 CO molecules was chosen for the vibrational analysis shown, see Table S12.

Table S12: Highest seven calculated CO vibrational frequencies for CO adsorbed on Pd in subnanometer cluster containing 10 Pd atoms ($Pd_{10}/CeO_2(111)$) and 7 CO molecules (using the scaling factor of 1.0085, see method section).

Pd_{10} & 7 CO	**Wavenumber / cm^{-1}**
Vib 1	1962
Vib 2	1950
Vib 3	1944
Vib 4	1931
Vib 5	1929
Vib 6	1922
Vib 7	1851

Table S13: Highest eight calculated CO vibrational frequencies for CO adsorbed on Pd in subnanometer cluster containing 10 Pd atoms ($Pd_{10}/CeO_2(111)$) and 8 CO molecules (using the scaling factor of 1.0085, see method section).

Pd_{10} & 8 CO	**Wavenumber / cm^{-1}**
Vib 1	2055
Vib 2	2051
Vib 3	2033
Vib 4	1941
Vib 5	1938
Vib 6	1906
Vib 7	1901
Vib 8	1886

Table S14: Highest nine calculated CO vibrational frequencies for CO adsorbed on Pd in subnanometer cluster containing 10 Pd atoms ($Pd_{10}/CeO_2(111)$) and 9 CO molecules (using the scaling factor of 1.0085, see method section).

Pd_{10} & 9 CO	**Wavenumber / cm^{-1}**
Vib 1	2074
Vib 2	2061
Vib 3	2040
Vib 4	2033
Vib 5	1933
Vib 6	1928
Vib 7	1911
Vib 8	1904
Vib 9	1891

Table S15: Highest ten calculated CO vibrational frequencies for CO adsorbed on Pd in subnanometer cluster containing 10 Pd atoms ($Pd_{10}/CeO_2(111)$) and 10 CO molecules (using the scaling factor of 1.0085, see method section).

Pd_{10} & 10 CO	**Wavenumber / cm^{-1}**
Vib 1	2072
Vib 2	2066
Vib 3	2053
Vib 4	2039
Vib 5	2034
Vib 6	1929
Vib 7	1909
Vib 8	1895
Vib 9	1828
Vib 10	1817

In situ / operando characterization

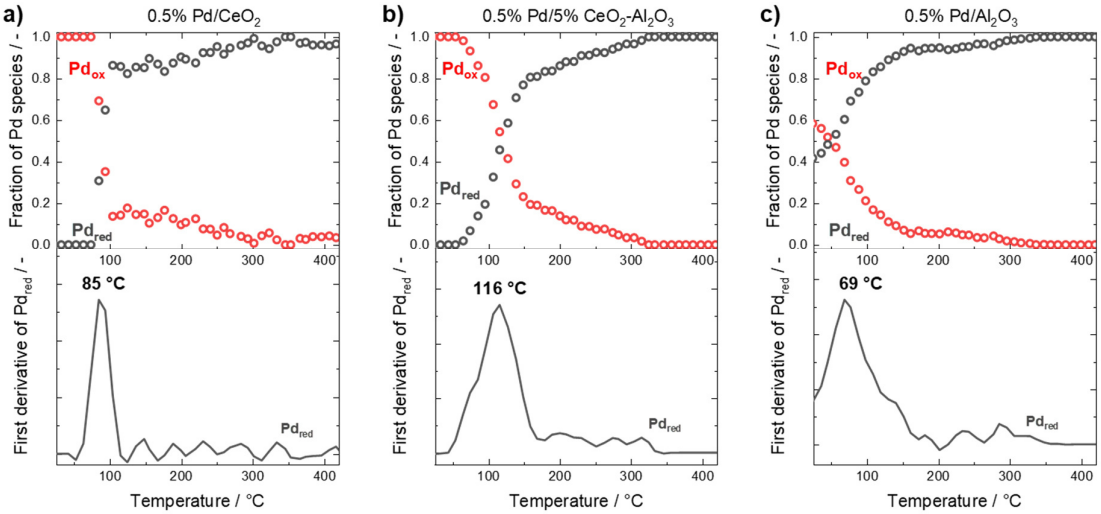

Figure S14: Results of the linear combination analysis of XANES spectra transiently recorded during H_2-Temperature-programmed reduction (TPR) in 2%H_2/He with a heating rate of 5 K min^{-1} for double-flame synthesized 0.5% Pd/CeO_2 (a), 0.5% Pd/5% CeO_2-Al_2O_3 (b) and 0.5% Pd/Al_2O_3 (c) with a corresponding first derivative of Pd_{red}. Due to large number of data points, the error bars are not shown to ensure clear data visualization. The LCA error is in the range of 1-3% for all samples.

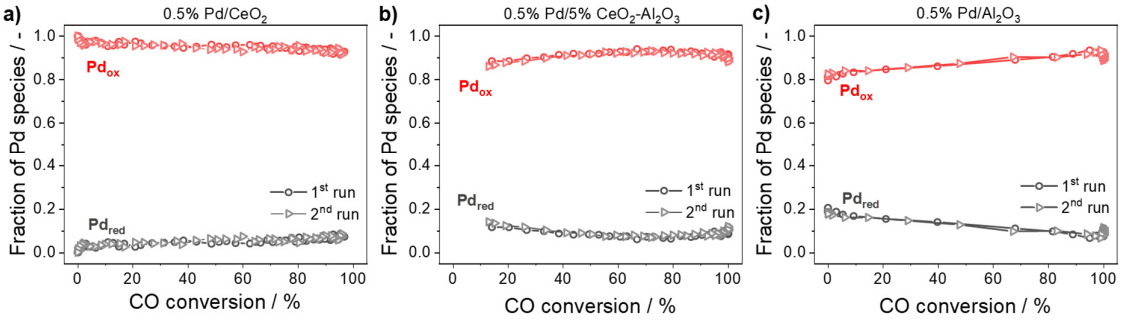

Figure S15: Results of the linear combination analysis of XANES spectra transiently recorded during cooling at the middle of the catalyst bed after two subsequent catalytic cycles in 1000 ppm CO/10% O_2/He with a cooling rate of 5 K min^{-1} for double nozzle-flame synthesized 0.5% Pd/CeO_2 (a), 0.5% Pd/5% CeO_2-Al_2O_3 (b) and 0.5% Pd/Al_2O_3 (c). Due to large number of data points, the error bars are not shown to ensure clear data visualization. The LCA error is in the range of 1-3% for all samples.

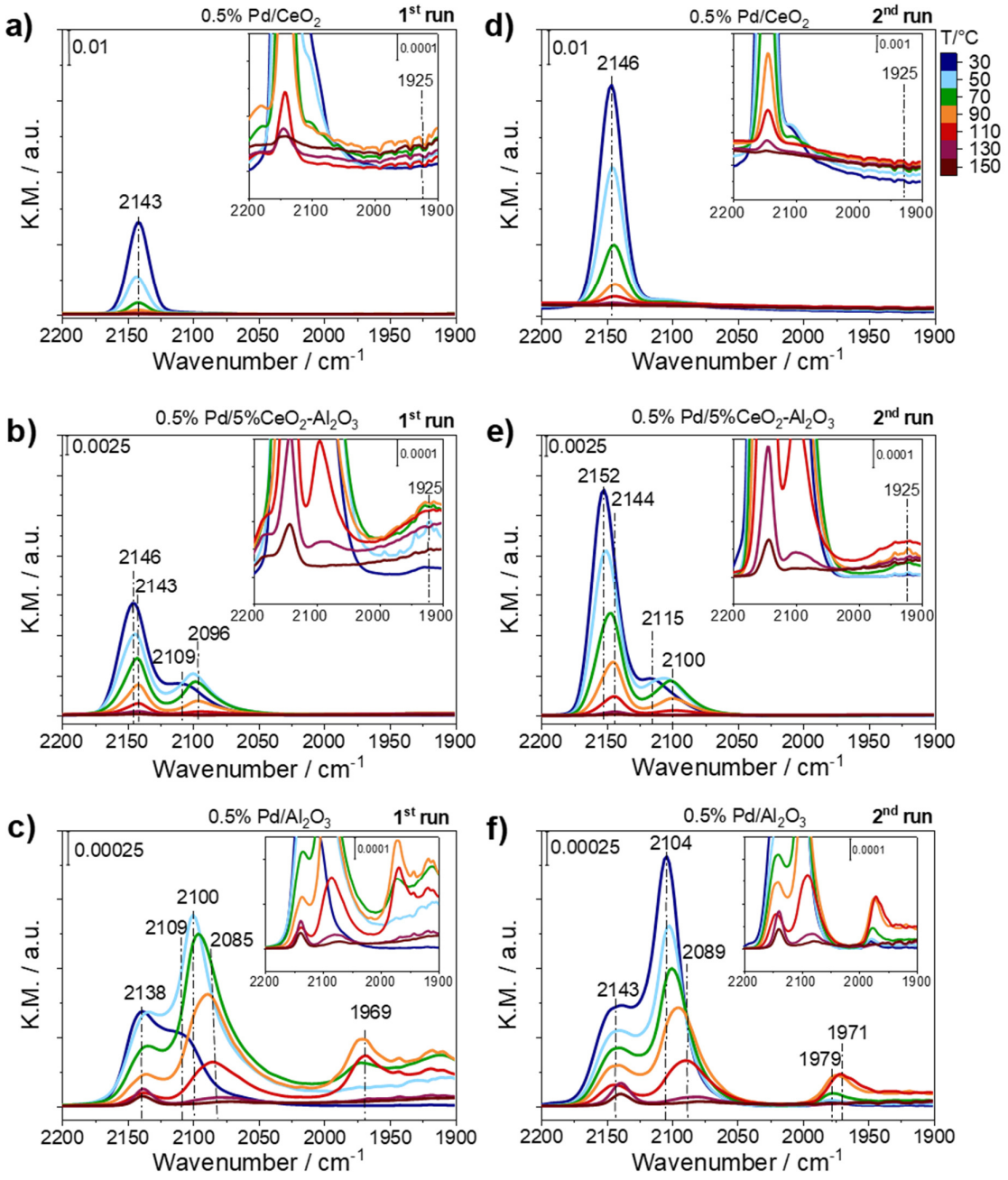

Figure S16: DRIFT spectra recorded during first (a-c) and second catalytic run (d-f) in 1000 ppm CO/10% O_2/He (200 mL min^{-1}) of double-nozzle flame synthesized 0.5% Pd/CeO_2 (a, d), 0.5% Pd/5% CeO_2-Al_2O_3 (b, e) and 0.5% Pd/Al_2O_3 (c, f) with a zoomed view of the 2200-1900 cm^{-1} region at different temperatures.

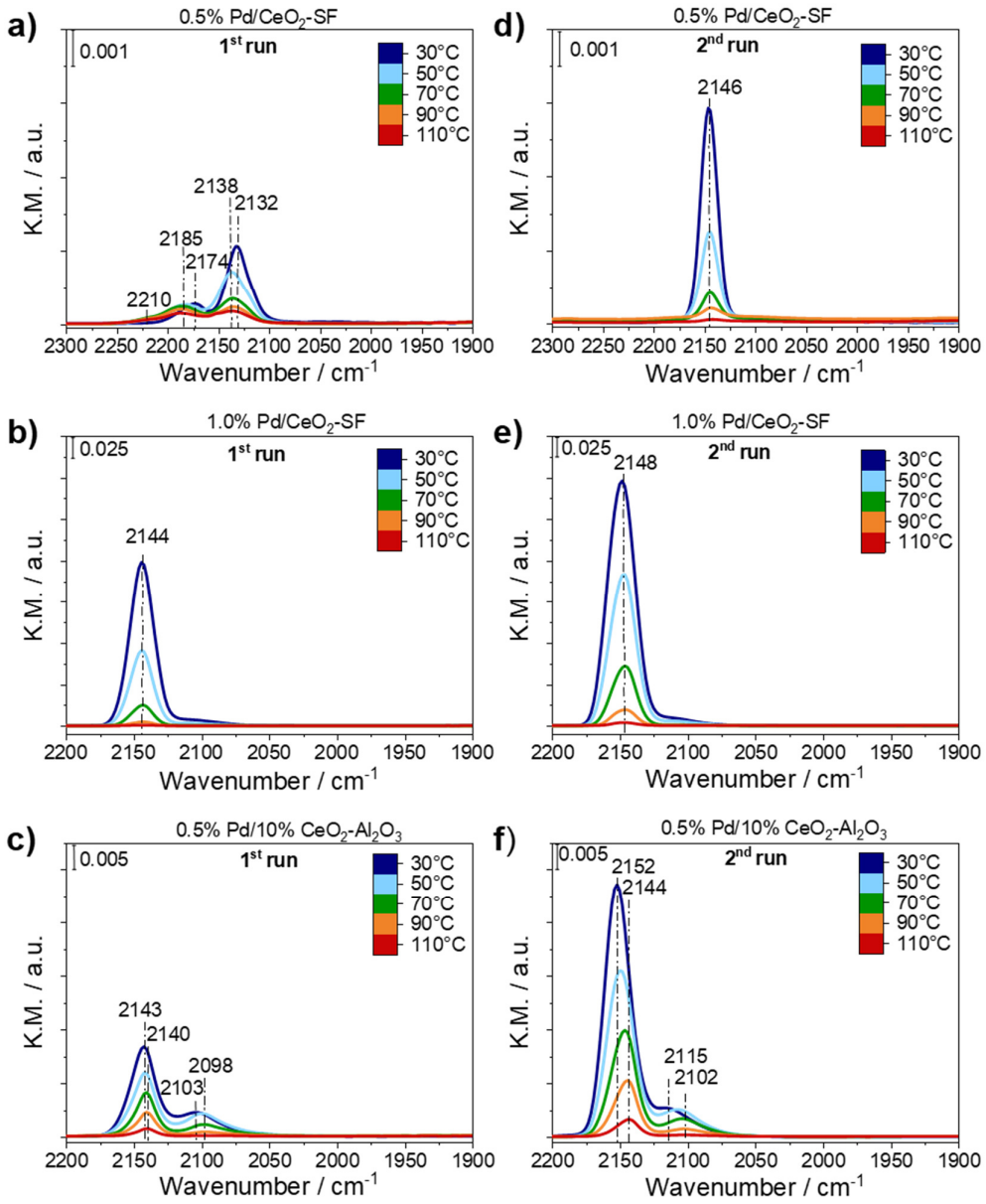

Figure S17: DRIFT spectra recorded during first (a-c) and second catalytic run (d-f) in 1000 ppm CO/10% O_2/He (200 mL min^{-1}) of 0.5% Pd/CeO_2-SF (a, d), 1.0% Pd/CeO_2-SF (b, e) and 0.5% Pd/10% CeO_2-Al_2O_3 (c, f).